Chemical Engineering Journal 534 (2026) 174823

Contents lists available at ScienceDirect

Chemical Engineering Journal

journal homepage: www.elsevier.com/locate/cej

In situ electrochemical remediation of real marine sediments polluted by PAHs and TPHs

Federica Proietto [a,*], Paola Meli [a], Andrea Di Franco [a], Flavia Gianfolcaro [a], Fabio D'Agostino [b], Alessandro Galia [a], Onofrio Scialdone [a]

[a] Dipartimento di Ingegneria, Università degli Studi di Palermo, Viale delle Scienze, Ed. 6, Palermo, 90128, Italy
[b] Istituto per lo studio degli impatti Antropici e Sostenibilità in ambiente Marino (IAS-CNR), Via del Mare 3, Torretta Granitola, TP, 91021, Italy

ARTICLE INFO

Keywords:
Marine sediments
TPHs
PAHs
Organic contents
Electrochemical remediation
Electrokinetic
Electrochemical geooxidation

ABSTRACT

In this work, real marine sediments from Bagnoli-Coroglio Bay (Naples, Italy), used as a model of real and complex matrix polluted by persistent organic pollutants, were treated by electrochemical process under a wide range of electric fields (*E*) (0.05–1.00 V cm^{-1}). Experiments were conducted using compact graphite electrodes directly inserted into the sediment for 96 h. The attention was focused on both TPHs and PAHs removal. Overall, this study demonstrates that electrochemical remediation (ER) applied to real marine sediments simultaneously promotes both the in situ *i*) desorption and transport of TPHs and PAHs and, also, *ii*) their chemical transformation, even under mild operating conditions. In detail, for all the applied *E*, a spatial redistribution of both TPHs and PAHs within the sediments bed was observed coupled with a partial removal of these compounds. This indicates that ER not only mobilizes contaminants but also promotes their oxidative transformation. Evidence of in situ transformation was supported by the formation of water-soluble organics. Furthermore, targeted analyses allowed to identify chloroacetic acids and low-molecular-weight carboxylic acids as major transformation products, whose formation and transport were *E*-dependent. Overall, results demonstrate that ER, even under mild *E*, enables both in situ desorption/transport and electrochemically driven transformation of hydrophobic contaminants in real sediments.

1. Introduction

Persistent organic pollutants (POPs) represent a major environmental concern due to their toxicity, resistance to degradation, and ability to bioaccumulate in marine ecosystems [1]. These compounds enter marine environments through multiple pathways. These include atmospheric deposition, land-based runoff, industrial discharges, and maritime activities, as well as from historical contamination linked to their past widespread use. Once introduced, POPs tend to adsorb onto fine-grained and organic-rich sediments, where they can persist for decades, acting as long-term sinks and secondary sources of pollution [2–6]. This persistence poses ecological risks to aquatic life and significant health hazards to humans through seafood consumption and environmental exposure. Addressing POP contamination in marine sediments therefore requires integrated strategies combining international regulation, continuous monitoring, and the development of effective remediation technologies [1]. The Italian government has designated 39 areas as Sites of National Interest (SIN) (MATTM, DM 2013). These sites are prioritized for environmental remediation because they contain high concentrations of hazardous contaminants, including lead, arsenic, mercury, and POPs such as polycyclic aromatic hydrocarbons (PAHs) and total petroleum hydrocarbons (TPHs). For instance, the marine sediments in Bagnoli-Coroglio Bay (Naples, Italy) have been classified as SINs due to extensive contamination linked to nearly 140 years of industrial activity (such as steel and cement production, chlor-alkali processing, fertilizer production, and crude oil refining) [7–10]. Currently, the management of contaminated marine sediments relies on techniques that are often inefficient, environmentally disruptive, time-consuming, and costly. Many of these conventional methods are also highly invasive, resulting in limited environmental and social sustainability [11]. For instance, phytoremediation requires extended treatment periods because the hyperaccumulation of pollutants by plants occurs slowly, making the process impractical for large-scale applications [12]. Similarly, bioremediation

* Corresponding author.
E-mail address: federica.proietto@unipa.it (F. Proietto).

https://doi.org/10.1016/j.cej.2026.174823
Received 2 December 2025; Received in revised form 29 January 2026; Accepted 2 March 2026
Available online 4 March 2026

is hindered by the limited mobility of microorganisms and by the inhibitory effects of toxic substances on their metabolic activity. Leaching processes, on the other hand, generate substantial amounts of secondary pollution, which must then be properly treated and disposed of [12]. Among the available remediation methods, electrochemical technology has emerged as an effective solution for treating contaminated sites with low hydraulic permeability, fine-grained sediments, complex heterogeneity, and mixed pollutants [13]. Electrochemical remediation (ER) offers several advantages over conventional techniques [14,15]. It can be applied ex situ or in situ and mobilize, transform, or extract contaminants that are otherwise difficult to remove. The method is environmentally friendly, avoiding the use of harmful solvents or chemical additives, and can be easily adapted for field applications. ER is also compatible with other treatment processes, non-invasive, and suitable for automation, requiring relatively simple equipment and addressing organic pollutant transformation at lower energy costs compared to traditional remediation methods [14,16]. ER technologies are versatile and effective for treating a wide range of pollutants in different soil and sediment types, particularly in low-permeability clays that contain adsorbed or dissolved contaminants [17]. Recently, several authors have shown that, among the electrochemical-based technologies, the electrochemical geo-oxidation (ECGO) process, which is conducted inducing a low electric field ($E \leq 0.25$ V cm^{-1}), is a suitable way to promote the desorption, transportation and also the transformation of organics in situ coupled with low energy consumption [14,15,17–22]. Zanko et al. successfully demonstrated the use of ECGO for treating in-situ polychlorinated biphenyl (PCB)-contaminated sediments from New Bedford Harbor (Massachusetts), achieving high removal efficiency over an operational period of about 1900 days [15]. Fan et al. demonstrated that electrochemical remediation of TPH-contaminated soil achieved about 22% removal after 80 days at 0.34 V cm^{-1}, mainly through electrochemical oxidation near electrodes and soil particles [20]. Saini et al. reported a 37% reduction of light TPHs (C10–C16) in BHP soil under 0.6 V cm^{-1} after one week [17]. Proietto et al. reached a total C12–C18 alkanes removal of ~70% using E of approximately 0.50 V cm^{-1} for 96 h [18]. More recently, Johansson et al. reported that ER using a pulsating direct low-current with alternating polarity is a suitable method for in situ degradation of PAHs in creosote-contaminated soil [23]. Proietto et al. provided the first evidence that, during electrochemical treatment at a low E of 0.15 V cm^{-1}, organic compounds undergo partial oxidation to form low-molecular-weight intermediates, such as carboxylic acids, ultimately leading to their mineralization [24]. Despite recent advances in ER, most studies have focused either on simplified matrices or on relatively high E intensities (typically 1.00–2.00 V cm^{-1}), often combined with chemical enhancers [25–28]. These conditions increase energy consumption (EC) and generate additional waste requiring treatment [25–28], and they rarely account for the behaviour of real sediments, where buffering capacity, heterogeneity, and contaminant mixtures strongly influence remediation performance.

Further efforts are needed to enhance the practical application of ECGO for remediating marine sediments contaminated with organic pollutants. Most existing studies mainly assess contaminant removal efficiency, neglecting the transformation pathways and the nature of intermediate byproducts. Marine sediments typically contain soluble salts, such as Na^+, Cl^- and smaller quantities of Mg^{2+}, SO_4^{2-}, K^+, Ca^{2+}. These ions may contribute to the generation of different reactive species and degradation mechanisms. Among them, Cl^- are of particular interest because they can be electrochemically oxidized to reactive chlorine species (such as ClO^-, HClO, Cl_2). These species may significantly alter in situ degradation pathways, leading to the formation of chlorinated byproducts. Key questions remain unresolved. In particular, the fate of TPHs or PAHs during in situ electrochemical treatment in real sediments is still poorly understood, especially regarding the formation, identity, and mobility of byproducts without clarifying whether byproducts were formed and whether these species might pose additional environmental risks. In contrast, this study focused on the ER applied directly to real marine sediments from the Bagnoli–Coroglio Bay (Naples), a site heavily contaminated with TPHs and PAHs. A preliminary study reported in the literature investigated the ER of these sediments focused exclusively on PAHs removal. The results showed that the treatment influenced both the removal and distribution of PAHs, confirming the potential suitability of this approach for remediating this type of matrix [19]. However, the experiments were performed only at an E of 0.05 V cm^{-1} without analysing the potential production of by-products. In the present study, attention was extended to both TPHs and PAHs removal. A systematic investigation was carried out to evaluate the effect of the E intensity (ranging from 0.05 to 1.00 V cm^{-1}) over an exposure time of 96 h. By coupling contaminant removal (R) with comprehensive byproduct identification (Total Organic Carbon (TOC) in pore water, chloroacetic acids (CAAs), carboxylic acids (CAs)) and EC analysis. This work provides new insights into the mechanistic pathways and practical feasibility of ER under mild operating conditions.

These results clarify how low-E treatments can simultaneously promote mobilization and transformation of TPHs and PAHs, identifying energy-efficient performance regimes suitable for in situ implementation. Overall, this study advances ER research by incorporating real-matrix behaviour, low-impact operating conditions, and detailed by-products profiling.

2. Material and methods

2.1. Chemicals

Calibration and method optimization of the GC–MS system were performed using a certified mixture of sixteen PAHs, including fluoranthene, chrysene, pyrene, acenaphthene, benzo(*k*)fluoranthene, anthracene, naphthalene, benzo(*b*)fluoranthene, dibenz(*a*,*h*)anthracene, benzo(*ghi*)perylene, acenaphthylene, phenanthrene, benzo(*a*)anthracene, indeno(1,2,3-*cd*)pyrene, benzo(*a*)pyrene, and fluorene purchased from CPAchem at a concentration of 2000 μg mL^{-1} each one. Deuterated internal standards (benzo(*a*)pyrene-D12, pyrene-D10, and acenaphthylene-D8) were also included.

Water HPLC grade (CAS 7732-18-5), acetone (HPLC grade, CAS 67–64-1) and acetonitrile (HPLC grade, CAS 75–05-8) supplied by Sigma-Aldrich were used for analytical apparatus and the extraction. n-Hexane (GC/MS grade, CAS 110–54-3) and compact graphite electrodes were obtained from Carlo Erba-Reagents.

KH_2PO_4 (CAS 7778-77-0), H_3PO_4 (CAS 7664-38-2), H_2SO_4 (CAS 7664-93-9) supplied by Sigma-Aldrich were used to prepare the eluent of HPLC analysis.

Standard of citric acid (CAS 77–92-9), acetic acid (CAS 64–19-7), fumaric acid (CAS 110–17-8), L-(+)-tartaric acid (TA, CAS 87–69-4), oxalic acid (OA, CAS 144–62-7), maleic acid (CAS 110–16-7), L-(−)-malic acid (CAS 97–67-6) and formic acid (FA, CAS 64–18-6), supplied by Sigma-Aldrich, were used to prepare the calibration curves for CAs in the HPLC method.

Phenol (PhOH, CAS 108–95-2, purity 99%), hydroquinone (CAS 123–31-9, purity >99%), 2-chlorophenol (2-CPs, CAS 95–57-8, purity >99%), 4-chlorophenol (4-CPs, CAS 106–48-9, purity >99%), 2,4-dichlorophenol (2,4-CPs, CAS 120–83-2, purity >99%), 2,6-dichlorophenol (2,6-CPs, CAS 87–65-0, purity >99%), 2,4,6-trichlorophenol (2,4,6-CPs, CAS 88–06-2, purity >99%), all supplied by Sigma-Aldrich, were used for the calibration curves of phenols and chlorophenols in HPLC analysis.

Mono (MCAA, CAS 79–11-8), di- (DCAA, CAS 79–43-6) and tri- (TCAA, CAS 76–03-9) chloroacetic acids standard analytical (Sigma-Aldrich) were used for the calibration curves of CAAs.

2.2. Marine sediments: sampling and characterization

Selected and utilized for their noted contamination and authentic

polluted marine sand from Bagnoli-Coroglio, in the southern part of Italy, near Naples (N 40°48.691′, E 14°09.755′). Marine sediments collected by grab sampling were stored in the dark at −20 °C for six months prior to characterization and treatment. This storage temperature minimizes compound volatilization and biological activity. Chemical analyses were conducted before electrochemical treatment to establish baseline conditions, ensuring that any minor speciation changes did not influence the results.

2.2.1. Grain size method

Grain-size analysis of the Bagnoli sand was carried out using an ASTM sieve stack with half-phi (ϕ/2) intervals, covering apertures from 2 mm (−1ϕ) to 63 μm (4ϕ), operated on a mechanical vibrating shaker. The resulting distributions were processed using the *Fritsch Particle Sizer AUTOSIEB/A20* software.

Following Krumbein (1934), particle sizes were classified according to the geometric Wentworth scale (1912) using the logarithmic phi (ϕ) transformation ($\phi = -\log_2 d$, where d is particle diameter in mm). Six independent duplicate measurements were performed to characterize the grain-size distribution. The granulometric characterization of the real marine sediments was summarized in Table 1.

2.2.2. PAHs and TPHs determination

A GC/MS to assess the concentration of the mixture of organic contaminants present in the real marine sediments of Coroglio-Bagnoli Bay was used. The quantification of individual PAH compounds in the superficial sediments was determined as follows. Sediment samples (1 g, dry weight) were placed in a glass test tube with 6 mL of n-hexane: acetone (80:20 v/v). Extraction was carried out using a high-frequency microwave sonication probe (HD 2070 SONOPULS, Bandelin, Germany) operating at 20 kHz, with a pulse cycle of 0.7 s ON and 0.3 s OFF, at 80% power for at least 10 min. After extraction, anhydrous Na_2SO_4 was added, and the mixture was vortex-mixed for 1 min. Centrifugation at 3000 rpm allowed recovery of the liquid phase. Purification of the extract was performed following EPA method 3630C, employing a Florisil SPE cartridge (200 mg/3 mL). The eluate was concentrated using a Büchi multi-vapor system, and the resulting residue was dissolved in 1 mL of n-hexane containing PAH-mix9 (deuterated internal standard, 200 μg mL^{-1}). Quantification of PAHs was carried out by GC/MS in SIM mode in accordance with the *EPA 8270D* protocol. The gas chromatograph was fitted with a DB5-MS capillary column (30 m × 0.25 mm × 0.50 μm). The experimental procedure for the GC/MS analysis involved setting the oven's temperature to 60 °C for a time of 4 min. Two heating ramps were applied: the oven was first brought to 270 °C at 10 °C min^{-1} and held for 5 min, followed by an increase to 340 °C at 20 °C min^{-1} with a final hold of 5 min. The temperature of the injector was set to 250 °C. The injection volume was 2 μL. The mean recovery rate of 16 prioritary PAHs, calculated on three replicate spiked sediments, was into the range of 83–91%. The limits of detection (LOD) and quantification (LOQ) were approximately 5 and 30 ppb for NAP, ACN, ACA, FLU, PYR and PHE, and 10 and 60 ppb for FLE, ANT, CHR, BBF, BJF, BAA, BPA, BPR, INP, DAN, respectively. Analytical uncertainty, evaluated using three PAH-spiked sediment samples at a concentration of 100 ppm, was into the range of 3 to 5%. The procedure for sample spiking is described in Ref. [19].

The determination of TPHs was carried out using a Thermo Scientific TRACE 1310 gas chromatograph equipped with a Programmed Temperature Vaporization (PTV) injector, a flame-ionization detector (FID), and a Thermo Scientific TriPlus RSH autosampler.

Chromatographic separation was achieved on a fast capillary column (10 m × 0.10 mm × 0.10 μm film thickness). The PTV injector operated in split mode (1:5) at a constant temperature of 270 °C, while the FID was maintained at 320 °C. Helium served as the carrier gas at a flow rate of 0.6 mL min^{-1}, and 2 μL of sample were introduced for each run. The oven program initiated at 80 °C with a 2-min isothermal hold, followed by heating to 350 °C at 30 °C min^{-1}, and a final 4-min hold at the maximum temperature.

The mean recovery rate of TPHs based on the total area of the chromatogram from C12-C40 was 87 ± 5% on three replicate spiked sediment samples. LOD and LOQ were approximately 0.5 and 3 ppm, respectively.

Table 1 reports the initial value of PAHs and TPHs of real marine sediments.

Table 1
Properties of natural marine sediments and contaminant TEC and PEC reference values.

Physical properties			SQSs [29]	
Physical properties		Bagnoli-Coroglio Bay	TEC[a]	PEC[a]
Specific gravity (at 20 °C)		2.58		
pH		7.20		
Moisture content (%)		37 ± 2.6		
Organic matter (%)		6.23 ± 0.02		
Particle size distribution (%)				
Clay		2.700 ± 0.2		
Silt				
Sand		97.4 ± 0.2		
Intrinsic ions in pore water (g/L)				
Cl^-		18.1 ± 2.2		
SO_4^{2-}		4.50 ± 0.2		
Na^+		17.7 ± 3.3		
$NH4^+$		0.08 ± 0.02		
K^+		0.90 ± 0.3		
Mg^{2+}		1.20 ± 0.9		
Ca^{2+}		0.40 ± 0.1		
PAHs[b] (μg kg^{-1})				
Naphthalene	NAP	–	–	–
Acenaphthylene	ACN	–	–	–
Acenaphthene	ACA	–	–	–
Fluorene	FLU	–	–	–
Pyrene	PYR	9100	195	1520
Fluoranthene	FLE	12761	423	2230
Phenanthrene	PHE	–	204	1170
Anthracene	ANT	1065	52.7	845
Chrysene	CHR	3947	166	1290
Benzo[b + k]fluoranthene	BBF	6477	–	–
Benzo[*j*]fluoranthene	BJF	1917	–	–
Benzo[*a*]anthracene	BAA	4603	108	1050
Benzo[*a*]pyrene	BAP	5911	150	1450
Benzo[*ghi*]perylene	BPR	4092	–	–
Indeno[1,2,3-*cd*]pyrene	INP	5190	–	–
Dibenz[*a,h*]anthracene	DAN	831	33	–
TPHs[b] (mg kg^{-1})				
Total Petroleum Hydrocarbons	TPHs	6957		

[a] The Probable Effect Concentration (PEC) indicates a contaminant level above which harmful effects on marine organisms are commonly expected, whereas the Threshold Effect Concentration (TEC) denotes the level below which adverse biological impacts are rarely observed.

[b] All these concentration values are the average of 10 replicated with a deviation standard close to 10%.

2.2.3. TOC in the pore water

Shimadzu VCSN ASI TOC-5000 analyzer was employed to quantify total organic carbon (TOC) in the pore water. For sample preparation, 1 g of wet sediment were weighed into a Falcon tube and mixed with 8 mL of deionized water. The suspension was vortexed for 5 min (ARGO-LAB vortex mixer) to ensure complete homogenization and then centrifuged at 4500 rpm for 20 min to separate the solid and liquid fractions. After decantation, the supernatant was filtered through a 0.2 μm nylon membrane filter to remove residual solids and subsequently analysed for TOC. TOC in the pore water was expressed relative to the dry sediment mass. The initial TOC (TOC°) was 60 ± 4 mg_C kg^{-1}.

2.2.4. Moisture, organic content, pH and ions characterization

As reported in the literature, the water content and organic fraction were determined according to ASTM D2974–14 method, whereas specific gravity was assessed in accordance with ASTM D854–92. Sediment

pH following the ISO 10390:2021 fixing a sediment/water ratio at 1:5 was determined. The pH was measured with a Checker® pH Tester (HI98103) supplied by HANNA® instruments. Moisture, which represents the water content (W), was calculated according to the method NF P 94–050.

Table 1 reports the initial value of moisture, organic content and pH of real marine sediments.

Soil buffering capacity measures the capacity of the solid to hold out an alteration in pH. The acid titration method was used to evaluate the acid buffering capacity. In particular, the initial pH of a suspension of sediment/water 1:5 was measured after a mixing by magnetic stirrer for 30 min. Then, the pH was measured after the addition of 1 mL of 0.1 M HCl every 60 min. This operation was iterated until the pH value was stable. Hence, pH values vs the amount of H^+ added per g of sediment (μmol g^{-1}) were plotted for the real marine sediments of Bagnoli-Coroglio Bay and kaolin (see Supporting Materials, Fig. S3). Data were discussed in qualitative form, by the comparison of the sediments with the kaolin (characterized by low acid buffering capacity).

Cl^- and SO_4^{2-} concentrations were analysed using ion chromatography (IC) on a Metrohm 882 Compact IC system equipped with a Metrosep® A Supp 5 anion-exchange column. The mobile phase consisted of 3.2 mM Na_2CO_3 and 1 mM $NaHCO_3$, delivered at a flow rate of 0.8 mL min^{-1}. The retention times were 5 and 14 min for Cl^- and SO_4^{2-}, respectively. Na^+, NH_4^+, K^+, Mg^{2+} and Ca^{2+} concentrations were analysed using a Metrohm 930 Compact IC system equipped with a Metrosep® C4 cation-exchange column. Temperature of the column was fixed at 45 °C. The mobile phase consisted of 0.5 mM oxalic acids and 4.5 mM nitric acid, delivered at a flow rate of 1 mL min^{-1}. The retention times were 6.4, 7.3, 9,5, 13.1, 15.4 min for Na^+, NH_4^+, K^+, Mg^{2+} and Ca^{2+}, respectively. 2 g of wet sediment were mixed with 10 mL of deionized water (1:5 ratio), vortexed for 3 min, allowed to reach equilibrium for 2 h under magnetic mixing at 200 rpm, and then centrifuged at 4000 rpm for 20 min. The resulting supernatant was filtered with 0.25 μm Nylon filter and subsequently analysed by IC. Moreover, this supernatant was used to measure the conductivity using a portable meter PC70Vio conductivity cell 2301 T. Initial porewater conductivity was 60 ± 5 mS cm^{-1}.

2.2.5. Characterization of the real marine sediments

Table 1 summarizes the physical and chemical properties of the marine sediments collected from Bagnoli–Coroglio Bay (Naples, Italy), as previously described in [19]. The material is composed predominantly of sand (about 97.4%). TPHs and PAHs concentrations were determined using ten sediment replicates, and the results are shown in Table 1. When compared with international Sediment Quality Standards (SQSs) [29], applicable to both marine and freshwater environments [30], the measured PAH levels surpass all benchmark limits, namely the Probable Effect Concentration (PEC) and Threshold Effect Concentration (TEC), by several orders of magnitude, indicating a likely harmful impact on aquatic organisms.

2.3. Electrochemical treatment

As done earlier by Proietto et al., electrochemical remediation was performed with an electrochemical set-up as shown in Fig. S1 of the Supplementary Material [19]. The cell is made of Plexiglass® cell and has an empty volume of 60 mL. A total of 66 g of contaminated sediment was introduced into the cell. To fill the cell, the sediments were introduced in successive layers. Each layer was pressed and gently vibrated to minimize void spaces. The packed sediment bed was then allowed to compact for 12 h. To prevent water evaporation, a Plexiglass® lid was placed on the cell.

This electrochemical treatment involves placing the electrodes directly into the sediment. Compact graphite electrodes were used as both anode and cathode; each electrode was a solid graphite bar with a width of 1 cm, height of 6 cm, and thickness of 3 mm. This material was selected for its high mechanical and chemical resistance and its good electrical conductivity. The electrodes were symmetrically positioned at a distance of 10 cm. The immersed active surface area of each electrode was 3 cm^2.

Before each treatment, three sediment aliquots already placed in the reactor were characterized for initial contaminant concentration, moisture content, and pH, since minor losses of water and volatiles can occur during sample preparation.

A constant cell voltage of 0.5, 1.5, 2.5, 5.0 or 10 V was applied with an Amel 2549 potentiostat/galvanostat at fixed electrode spacing of 10 cm, inducing a constant direct E with interval 0.05–1.00 V cm^{-1}. As a result, E was effectively constant for each experiment, while the current evolved over time in response to changes in the overall sediment conditions. Each electro-remediation was conducted for a duration of 96 h in ambient conditions. Temperature of the sediment bed was measured using a RS 206–3722 thermometer equipped with a K-type thermocouple. To ensure reproducibility, each experiment was conducted in duplicate. Sediment samples were collected from three locations within the reactor (Fig. S1): S1 near the anode, S2 in the middle section, and S3 close to the cathode. At the end of the treatment, three sediments section from the cell were extracted. Contaminants, by-products, pH, and moisture were quantified following the procedure described in other sections. All determinations were run in triplicate, and average values are presented.

Additionally, control experiments were carried out in the absence of an applied E for a total duration of four days. In these tests, approximately 83–92% of the initial PAHs and TPHs content were recovered, aligning with the study's objectives. The small discrepancy in mass balance may be attributed to losses due to volatilization and/or adsorption of PAHs and TPHs onto components of the electro-remediation setup (e.g., electrodes, vials, and cell surfaces).

2.4. Water-soluble organics analytical methods

To identify and quantify by-products formed during electrochemical treatment, HPLC analysis was performed using an Agilent 1260 system.

The concentrations of CAAs (MCAA, DCAA, and TCAA) were determined using an HPLC (Agilent 1260) using a Kinetex C18 column (5 μm, 100 Å, 150 × 4.6 mm; Phenomenex). Separation was achieved with a 25 mM KH_2PO_4 solution adjusted to pH 2.5 as the mobile phase, delivered at a flow rate of 0.5 mL min^{-1}. Detection was performed at 210 nm, and 10 μL of each sample was injected. The retention times were 5.6, 4.6 and 8.4 for MCAA, DCAA and TCAA, respectively. For CAAs, LOD and LOQ were 2 and 6 mg kg^{-1} for MCAA, 1 and 3 mg kg^{-1} for DCAA and 2.5 and 7.5 mg kg^{-1} for TCAA, respectively.

CAs were quantified using an Agilent Infinity 1260 HPLC system equipped with a Luna Omega Polar C18 column (3 μm; Phenomenex) coupled to a UV detector set at 210 nm. The mobile phase was a 100 mM aqueous KH_2PO_4 solution (HPLC grade), adjusted to pH 2.5 with H_3PO_4, and operated at 25 °C with a flow rate of 1.0 mL min^{-1}. Calibration curves were obtained using analytical standards for various CAs. The retention time were 2.67 min for oxalic acid, 3.25 min for L-(+)-tartaric, 3.55 min for formic acid, 4.37 min for L-(−)-malic acid, 5.85 min for acetic acid, 7.26 min for maleic acid, 8.7 min for citric acid and 9.4 min for fumaric acid. For CAs, LOD and LOQ were 2 and 6 mg kg^{-1} for oxalic acids, 0.5 and 1.5 mg kg^{-1} for tartaric acids and 1 and 3 mg kg^{-1} for formic acid, for 2 and 6 mg kg^{-1} L-(−)-malic acid, 5 and 15 mg kg^{-1} for acetic acid, 0.6 and 1.8 mg kg^{-1} for maleic acid, 6 and 18 mg kg^{-1} for citric acid, 2.5 and 7.5 mg kg^{-1} for fumaric acid, respectively.

Phenol, chlorophenols, and hydroquinone were quantified by HPLC (Agilent 1260) using a Kinetex C18 column (5 μm, 100 Å, 150 × 4.6 mm; Phenomenex). UV detection was performed at 214 nm. The mobile phase (acetonitrile/water) was maintained at 25 °C with a flow rate of 1.0 mL min^{-1}. Separation was achieved through a gradient elution, starting from 20/80% v/v acetonitrile/water at 0 min to 95/5% v/v at 5 min. Calibration curves were obtained using analytical standards of each

compound. The retention time were 1.9 min for hydroquinone, 3.8 min for PhOH, 4.6 min for 2-CPs, 4.7 min for 4-CPs, 5.3 min for 2,4-CPs, 5.15 min for 2,6-CPs, and 5.8 min for 2,4,6-CPs. For phenols, chlorophenols and hydroquinone, LOD and LOQ were 0.02 and 0.05 mg kg^{-1}, respectively.

All analyses were conducted in triplicate, yielding an analytical uncertainty below 3%, indicating good reproducibility.

The by-products concentrations (mg L^{-1}) were normalized and expressed as mg of each acid per kg of dry sediment mass ($mg_{i\text{-byproducts}}$ kg^{-1}).

2.5. Performances

At the end of each treatment, the distribution of each contaminant (*i*) across sediment sections S1, S2, and S3 was assessed by calculating the ratio between its final concentration (C_i) and its initial concentration (C°_i). To verify that contaminants were evenly distributed before starting the experiments, sediment samples were collected from S1, S2, and S3, dried, and analysed following the procedure described above. At time zero, the initial concentrations of all contaminants were essentially uniform, with $C_i/C_i^{\circ} \sim 1 \pm 0.08$.

The removal efficiencies for TPHs and PAHs were determined using eqs. 1 and 2:

$$R_{TPHs} = \frac{\left(C^0_{TPHs} - C^t_{TPHs}\right)}{C^0_{TPHs}} * 100[=]\% \quad (1)$$

$$R_{PAHs} = \frac{\left(C^0_{PAHs} - C^t_{PAHs}\right)}{C^0_{PAHs}} * 100[=]\% \quad (2)$$

where C_i^0 is the initial concentration of TPHs or PAHs and C_i^t is their residual amount after 96 h, both normalized to the dry mass of the treated sediments (mg kg^{-1}). Hence, the R reflects the decrease in the total mass of a given contaminant in the treated sediment (sum over S1–S3) relative to its initial mass in the cell.

Energetic consumption (EC) was evaluated according to eq. (3):

$$EC = \frac{I * \Delta V * t}{w} * 10^{-3}[=]\, kWh\, kg^{-1} \quad (3)$$

where I is the time-integrated current (A), ΔV the constant applied voltage (V), t treatment duration (h) and w is total dry mass of processed sediments (kg).

3. Results and discussion

In this study, real marine sediments from Bagnoli-Coroglio Bay (Naples, Italy) were treated by electrochemical process using electrodes placed in direct contact with the sediments and without adding enhancing agents. The main aim of this study was to evaluate the remediation potential of the ER under a wide range of E when a real and complex matrix (Bagnoli-Coroglio Bay's sediments) was used. In this study, the electrochemical treatment applied to marine sediments is framed within the broader category of ER. When operated under low E ($\leq$ 0.25 V cm^{-1}), the process also aligns with the concept of ECGO. Because the present work investigates a wider range of E intensities, including values above the typical ECGO domain, the term ER is adopted throughout the manuscript as the standard descriptor. The term ECGO is used only when specifically referring to low-E conditions or when comparing our results with studies that explicitly adopt this terminology. Moreover, to facilitate the interpretation of the profiles reported in the next sections, it is important to distinguish the different processes governing contaminant behaviour under ER. First, the C_i/C_i^0 gradients observed across S1–S3 reflect internal redistribution, mainly driven by transport mechanisms, and do not represent removal. Second, mobilization into pore water is captured by TOC measurements, which reveal solubilisation or the formation of more polar intermediates. Third, chemical transformation is inferred from the appearance of identifiable oxidation products (e.g., lower-molecular-weight organics), indicating that part of the contaminant mass is converted into lower-molecular-weight species rather than simply displaced. Finally, the removal efficiency (R) refers exclusively to the net decrease in the total contaminant mass within the cell (sum of S1–S3) relative to the initial load and therefore reflects a true loss of contaminants from the sediment matrix.

3.1. Electrochemical remediation of real marine sediments

In order to investigate the ER of contaminated real marine sediments, a set of experiments was performed under low E value of 0.25 V cm^{-1} for 96 h. Electrolyses were carried out using graphite electrodes, which were directly placed inside the sediments. Process' performances were estimated in terms of the normalized concentration of the total TPHs, each PAHs, the total PAHs (C_i/C_i^0) as well as their total removal efficiency (R_i). Fig. 1 reports the treatment's results of TPHs (1A), total PAHs (ΣPAHs) (1B), each PAHs (1C) in the sections S1, S2 and S3 and the total R_i (1D). The dashed black line in the Fig. 1A - C represents the zero time where the C_i/C_i^0 ratio is ~1, showing that the contaminants are homogeneously distributed inside the electrochemical cell. After 96 h, comparable trends were observed for both TPHs and ΣPAHs (Fig. 1A and B, respectively). In the case of TPHs, the C_i/C_i^0 ratio reached its minimum value in section S1 and progressively increased toward sections S2 and S3. For ΣPAHs, the lowest values were observed in sections S1 and S2, while the highest occurred in section S3. Specifically, it was found that, for all PAHs, the spatial distribution of each contaminant within the sediments exhibited a comparable pattern (Fig. 1C): the *i*-contaminant concentration was lower in regions S1 (anode area) and/or S2 (middle area), and consistently higher in S3 (cathode area).

In ER of contaminated sediments, the transport of water, ions, and colloidal particles through fine-grained media predominantly occurs via electromigration and electroosmosis [31,32]. These mechanisms facilitate the movement of pollutants from the area closer to one electrode toward the opposite side. In the present study, the contribution of electromigration to the mobility of the TPHs and PAHs can be considered negligible due to their non-polar nature. Consequently, the electroosmotic flux directed toward the cathode could justify the highest TPHs and PAHs concentrations detected in the cathodic zones (S3). Nonetheless, the overall electroosmotic transport is expected to be limited, given the hydrophobic character and low solubility of both TPHs and PAHs. These findings are consistent with our previous study on marine sediments spiked with five model PAHs [19]. Moreover, the observed spatial redistribution can also be influenced by the intrinsic heterogeneity of the real marine sediments, including variations in grain size distribution, mineralogical composition, organic matter content, and porosity across the sediment bed. Fine-grained and organic-rich domains are known to enhance the sorption of hydrophobic contaminants, such as PAHs and TPHs, potentially leading to localized retention and reduced mobility. As a result, sediment heterogeneity may modulate electroosmotic transport efficiency, contributing to non-uniform contaminant redistribution along the matrix.

It is worth to mention that, under the applied experimental conditions (E of 0.25 V cm^{-1} for 96 h), an overall R greater than zero was reached for both TPHs and PAHs (Fig. 1D). The R of TPHs and ΣPAHs reached approximately 10 and 23%, respectively. In the latter case, a distinct inverse relationship was observed between the removal efficiency and the molecular weight of the PAHs: as the number of aromatic rings increased, the removal rate generally decreased. The compounds could be grouped according to their removal behaviour as follows: C22 compounds (DAN $C_{22}H_{14}$, INP $C_{22}H_{12}$, BPR $C_{22}H_{12}$) < C20 compounds (BBF $C_{20}H_{12}$, BKF $C_{20}H_{12}$, BAP $C_{20}H_{12}$) < C14–18 ones (ANT $C_{14}H_{10}$, FLE + PYR $C_{16}H_{10}$, BAA $C_{18}H_{12}$, CHR $C_{18}H_{12}$) (Fig. 1D). These findings suggest that, besides the electroosmotic transport of TPHs and PAHs, additional transformation pathways contributed to their degradation. In particular, given the strong affinity of PAHs and TPHs for sediment

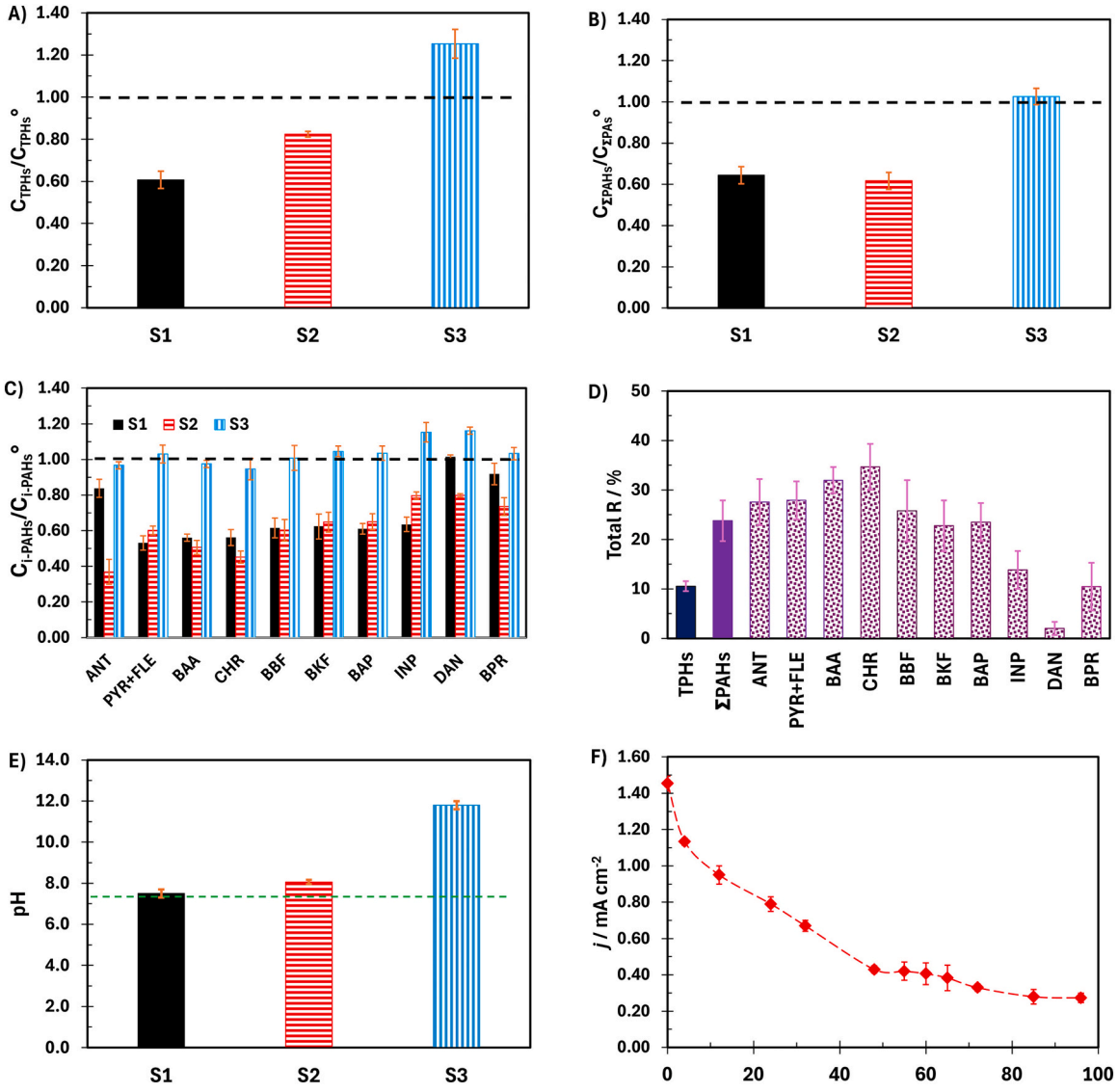

Fig. 1. Effect of the electrochemical remediation of real marine sediments of Bagnoli Bay under 0.25 V cm^{-1} on the normalized concentration of (A) TPHs, (B) ΣPAHs, and (C) each detected PAH (ANT, FLE + PYR, BAA, CHR, BBF, BKF, BAP, INP, DAN, BPR) in the region S1, S2 and S3 after 96 h. (D) Total removal of TPHs, ΣPAHs, ANT, FLE + PYR, BAA, CHR, BBF, BKF, BAP, INP, DAN and BPR from the sediment. (E) Plot of the pH in the region S1, S2 and S3 after 96 h. (F) Plot of current density (*j*) vs. time during the ER treatment. Error bars indicate the standard deviation calculated from two independent experiments. The dashed black line in the Figures A, B and C represents the zero time where the C_i/C_i^0 ratio is ~1. The dashed green line in the Figure E represents the pH at the zero time.

particles, particle-associated reactions occurring at the sediment–pore water interface likely played a relevant role.

Previous studies have suggested that, during ER under low *E*, various reactive species are generated in situ at the anode or in proximity to sediment particles. These reactive species include hydroxyl radicals (•OH) formed through water anodic oxidation, hydrogen peroxide produced via oxygen cathode reduction, and active chlorine species arising from NaCl anodic oxidation (E° = 0.99, 0.89, 0.76 and 0.64 V vs SCE at pH 7, 10, 12 and 14, respectively) (Eqs. 4–6) [33]. The formation of these oxidants promotes the transformation of organic contaminants [14,18,19].

$$2Cl^- \rightarrow Cl_2 + 2e^- \qquad pH < 3 \tag{4}$$

$$Cl_{2\ (aq)} + H_2O \rightarrow HClO + Cl^- + H^+ \qquad 3 < pH < 8 \tag{5}$$

$$HClO \rightarrow ClO^- + H^+ \qquad pH > 8 \tag{6}$$

Chloride in the system originates from the intrinsic salinity of the marine sediment and pore water characteristic of the Bagnoli–Coroglio coastal environment. Pore water analysis by ion chromatography confirmed the presence of elevated Cl^- concentrations (Table 1: 18.1 ± 2.2 g/L with a measured initial pore water conductivity of 60 ± 5 mS cm^{-1}), supporting the occurrence of active chlorine pathways. Moreover, the formation of active chlorine species during ER using low *E* has been previously demonstrated treating alkanes-contaminated kaolin [18]. In addition, the direct placement of graphite electrodes within the sediment matrix enhances electrode–sediment interactions, leading to the formation of localized electrochemically active zones. At the electrode–sediment interface, steep redox are expected to develop, promoting direct anodic oxidation of particle-bound contaminants or their reaction with short-lived oxidizing species generated in situ. These localized processes may contribute to the preferential depletion of PAHs and TPHs observed in the anodic (S1) and central (S2) sections. Although the exact mechanisms are not yet fully understood, PAHs and TPHs, for example, are known to react readily with hydroxyl radicals, forming a range of oxygenated or partially oxidized intermediates [34–37]. In addition, direct electrochemical oxidation may occur at the anode surface under the adopted conditions as previously shown for the

electrochemical wastewater treatment. Literature evidence indicates that anodic oxidation of PAHs may proceed either through direct electron transfer from adsorbed PAH molecules to the electrode, forming reactive PAH radicals that subsequently undergo further reactions [35,38], or via oxidation by in situ obtained hydroxyl radicals. For instance, Alcántara et al. (2008) reported complete degradation of BAP, PHE, and ANT in water media using graphite within three days, emphasizing that the underlying mechanisms remain complex and not yet fully elucidated [39]. Chen et al. reported a total TPHs removal of 45% after 300 min of a H_2O_2-based-Fenton technologies, due to the generation of hydroxyl radicals [36]. In this context, it is noteworthy that recent findings have shown that, under low *E* conditions, organic compounds can undergo in situ transformation into lower-molecular-weight products, eventually leading to mineralization [24].

The initial pH was estimated to be 7.20. After the electrolysis process, a spatial variation in pH was observed: it slightly increased from S1 (7.25) to S3 (11.8) (Fig. 1E). This pattern is consistent with findings reported in the literature, wherein pH variations under similar experimental conditions are due to the pore water electrolysis occurring at the electrode interfaces. The used cell potential was sufficient to induce water electrolysis [40]. Consequently, water oxidation and reduction lead to the generation of H^+ ions and OH^- ones at the anode and the cathode, respectively [40]. Here, in opposite with the literature, the pH value at the anode side (S1) does not decrease after the treatment due to the production of H^+; the effect can be attributed to the fact that Bagnoli-Coroglio sediments are characterized by a high acid buffer capacity, which might hinder the movement of H^+. To clarify this aspect, additional chemical tests were conducted by adding controlled amounts of acid to the sediments and allowing the system to reach equilibrium. The results showed that the pH of the Bagnoli–Coroglio sediments changed only slightly upon H^+ addition (Supporting Materials, Fig. S3), confirming their high buffering capacity. It is therefore reasonable to assume that the migration of H^+ toward the cathode (acid front) is hindered by this strong buffering effect, consistent with our previous findings [19].

It is important to underline that electrokinetic treatments carried out under relatively high *E* strengths (i.e., > 1.00 V cm^{-1}) often trigger considerable electric current flow in saline soils or sediments because of their naturally high electrical conductivity. Such conditions can lead to undesirable side effects, including localized overheating, moisture depletion, and increased consumption of energy and process fluids [41]. In this work, the application of low *E* of 0.25 V cm^{-1} resulted in a gradual decline of current density (*j*) during the initial treatment phase, reaching an almost stable value of approximately 0.27 ± 0.04 mA cm^{-2} after 70–96 h (Fig. 1F) coupled with an energetic consumption of 3.95 10^{-3} kWh kg^{-1}. Under these operating conditions, and as confirmed by previous studies, temperature fluctuations within the sediment can be considered negligible [14,26,42]. During the experimental period, the temperature remained constant at approximately 22 ± 1 °C. This observation suggests that maintaining a low-intensity *E* is not only effective in promoting the electrochemical transformation of organic compounds but also advantageous in preserving the physical integrity of the sediment by avoiding thermal stress, moisture reduction and excessive EC.

The Bagnoli–Coroglio sediments contain both organic pollutants and heavy metals (Pb, As, Zn and Hg), which may theoretically influence ER performance through adsorption on electrode surfaces, partially altering the availability of reactive sites or the competition for reactive oxidants (such as hydroxyl and chlorine-based radicals). In addition, pH and redox changes induced by the applied *E* can modify metal speciation and mobility, potentially affecting desorption and transformation pathways of PAHs and TPHs. Although metals were not monitored in this study, our previous work on real Bagnoli sediments showed that low *E* (≤ 0.25 V cm^{-1}) did not modify arsenic concentrations or distribution ($C_i/C_i^0 \sim 1$), indicating its limited mobilization under these conditions [19]. Future studies should investigate more in detail the potential effect of metals on organics' removal in mixed-contaminant marine sediments.

In this study, to optimize the operational parameters, the subsequent tests focus on the influence of the *E* intensity on organics contaminants distribution and their removal within the sediment bed.

3.2. Effect of the E values

The intensity of the applied *E* can markedly influence the remediation process. Therefore, a series of electrolysis experiments was designed to evaluate the effect of different *E* strengths on the treatment of real marine sediments. Figs. 2 reports the C_i/C°_i of TPHs and ΣPAHs, within the sections S1, S2 and S3 (Fig. 2A and C) and their relative R (Fig. 2B and D), respectively, over 96 h under varying *E* values (range: $0.05 \div 1.00$ V cm^{-1}). Overall, the change in *E* determines a variation in both the spatial distribution and the total R. Focusing the attention on TPHs, the change of *E* slightly affects the qualitative spatial distribution of the TPHs; in most of the cases, they presented the lowest and the highest concentrations in sections S1 and S3, respectively, due to the mechanisms above discussed. For all *E*s, the C_{TPHs}/C°_{TPHs} ratios were lower than 1 in S1 and S2 (Fig. 2A). Moreover, at the lowest and highest *E* values (0.05 and 1.00 V cm^{-1}, respectively), the C_{TPHs}/C°_{TPHs} ratios were lower than 1 also in S3 (Fig. 2A). Across the entire *E* range examined, appreciable values of R_{TPHs} were recorded. The dependence of R on *E* exhibited a clear minimum close to 10% at 0.25 V cm^{-1} (Fig. 2B). At the lowest and the highest *E* tested (0.05 and 1.00 V cm^{-1}), the total R_{TPHs} reached approximately 16 and 26%, respectively (Fig. 2B). Very similar trends were observed in the case of PAHs removal. A clear dependence of the C_{PAHs}/C°_{PAHs} and R_{PAHs} were achieved by changing the adopted *E*. In most of the cases, ΣPAHs presented the lowest and the highest concentrations in sections S1 and S3, respectively (Fig. 2C). In this case, it was observed that the C_{PAHs}/C°_{PAHs} ratios were lower than 1 in all the sections under all the applied *E* (Fig. 2C). The detailed effect of the *E* on the spatial distribution of each PAH after the ER over 96 h was reported in Fig. S2 (see Supplementary Material). Fig. 2D reports the $R_{\Sigma PAHs}$ at various adopted *E*s. As in the case of TPHs, a trend with a minimum for $E = 0.25$ V cm^{-1} was observed and at the lowest and highest *E* values (0.05 and 1.00 V cm^{-1}, respectively), a $R_{\Sigma PAHs}$ of approximately 39 and 59% was recorded, respectively (Fig. 2D). These results shown that the effect of *E* on the removal of both TPHs and PAHs is very similar, although higher abatement levels were achieved for PAHs across the entire range.

To rationalize these data, it is relevant to consider the following points.

- When the *E* exceeds 0.25 V cm^{-1}, increasing *E* results in a higher electric current (rising from 0.27 to 0.46 mA cm^{-2} at 0.25 and 1.00 V cm^{-1}, respectively). This boosts the driving force of the electrochemical reactions, potentially accelerating the generation of reactive radicals and/or oxidant, and consequently speeding up the transformation of TPHs and PAHs.
- The positive results achieved by decreasing the *E* values to 0.05 V cm^{-1} may be linked to the fact that, at 0.25 V cm^{-1}, electrical current is partially transmitted through sediments particles and partially through the pore fluid [43]. Under these conditions, sediments particles can behave as microelectrodes, facilitating redox reactions at the diffuse double layer (DDL) interface. A decrease in the *E* strength likely reduces the proportion of ionic current in the pore solution while enhancing electron transport through the solid phase [44,45]. This shift promotes more intense redox activity at the DDL [15], thereby increasing the generation of reactive radical species on particle surfaces that drive the in situ chemical reactions. This is a mechanistic interpretation consistent with the literature but not directly measured in this work. To support this interpretation, future studies should monitor additional parameters, such as local conductivity, potential distribution or electroanalytical characterizations.

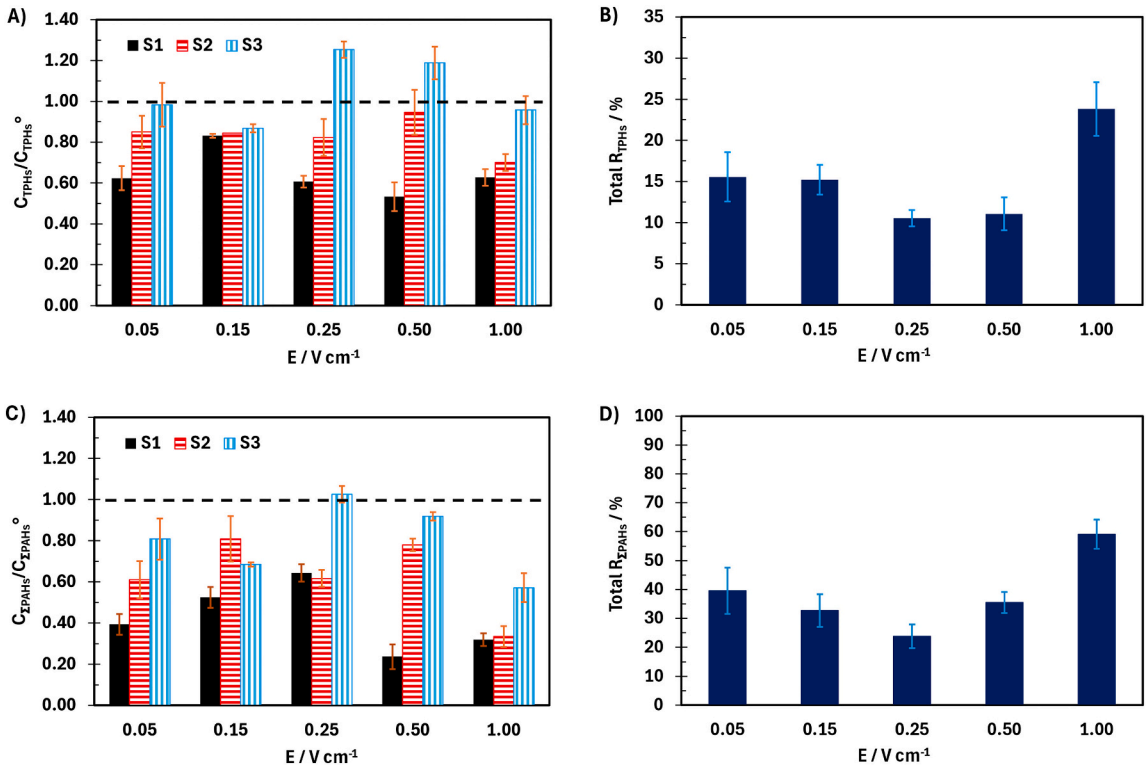

Fig. 2. Effect of E ranged from 0.05 to 1.00 V cm^{-1} on the (A) TPHs and (C) ΣPAHs in the section S1, S2 and S3 and (B) the total R_{TPHs} and (D) $R_{\Sigma PAHs}$ after 96 h of electrochemical treatment. Electrolyses were performed for 96 h. Error bars indicate the standard deviation calculated from two independent experiments. The dashed black line in the figures A and C represents the zero time where the C_i/C_i^0 ratio is ~1.

Overall, these findings indicate that both lower and higher E strengths than 0.25 V cm^{-1} can enhance TPHs and PAHs removal through different, E-dependent electrochemical and pH-related mechanisms, with lower E values offering the added advantage of reduced EC. Indeed, EC increases with the E intensity: from 1.90 10^{-7} to 3.95 10^{-3}, and 22 10^{-3} kW h kg^{-1} under 0.05, 0.25, and 1.00 V cm^{-1}.

Moreover, the E value affects the sediments pH. Within the 0.25–1.00 V cm^{-1} range, increasing the applied E caused the pH in section S1 to drop steadily from 7.25 to 4.00, while in section S3 it rose slightly from 11.8 to 12.0 (Fig. 3). In contrast, the pH in the central section (S2) remained essentially unchanged (Fig. 3). Previous studies indicate that the acidic front generated at the anode is transported toward the cathode by both electroosmosis and electromigration [43], while the hydroxide ions formed at the cathode migrate toward the anode, moving against the electroosmotic flow. In addition, protons are known to travel through sediments more rapidly than hydroxyl ions. Therefore, within the E range of 0.25–1.00 V cm^{-1}, a stronger E, and consequently a higher current, can enhance ion electromigration. This results in lower pH values near section S1 and higher pH values near section S3. At relatively elevated E intensities ($\geq$ 0.25 V cm^{-1}), the faster proton mobility combined with intensified electromigration enables protons to influence and moderate the pH even in section S3 (indeed, the pH values decrease always with the E (Fig. 3; pH S1). These change in pH could affect the organics' desorption and the main processes involved in their in-situ transformation. Conversely, for E < 0.25 V cm^{-1}, no appreciable shifts in sediment pH were detected, due to its high acid-buffer capacity which hinders the movement of H^+ (see Supporting Material, Fig. S3).

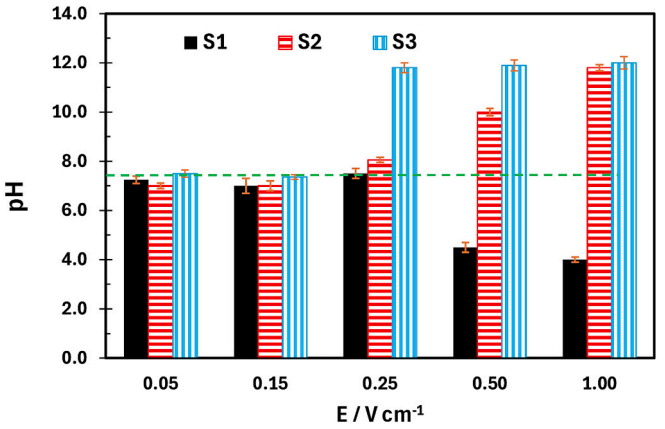

Fig. 3. Effect of the E on the pH in the sections S1, S2 and S3 after 96 h. Error bars indicate the standard deviation calculated from two independent experiments. The dashed green line represents the pH at the zero time.

When compared with previous ER studies conducted on real sediments or soils under low E, the removal efficiencies achieved in this work fall within the same order of magnitude. For instance, Zanko et al. [15] reported substantial PCB attenuation in real harbor sediments (R > 90%) operated at $E \leq$ 0.25 V cm^{-1} over treatment periods extending to several years. Similarly, Fan et al. [20] and Saini et al. [17] observed TPH removals of approximately 20–40% in real soils under low to moderate Es (0.34–0.60 V cm^{-1}, respectively) after weeks to months of treatment. Very similar removal levels for real sediments were reported in our previous study, in which a total PAHs removal efficiency of about 57% was achieved in real marine sediments from Augusta Bay (Italy) under a low E of 0.05 V cm^{-1}, confirming that appreciable PAHs attenuation can be obtained even under very mild operating conditions [19]. Under comparable E conditions, the present results show comparable PAHs and TPHs abatements in real marine sediments.

3.3. Effect of the electrochemical remediation on chemical transformation of TPHs and PAHs

3.3.1. Total organic carbon in pore water

TPHs and PAHs have very low solubility in water and therefore tend to accumulate in sediments and soils. Only a small portion, known as the water-soluble fraction (WSF), is present in the aqueous phase, typically composed of the more soluble aromatic compounds. To assess if ER influences the formation of water-soluble organics (WSO), a systematic study was conducted focusing on the quantification of the total organic carbon (TOC) in the pore water. The initial TOC (TOC°) of the wet sediments was estimated to be approximately 60 $mg_C\ kg^{-1}$.

Fig. 4 shows the normalized TOC values in S1, S2, and S3 after ER over a wide range of *E*. The dashed black line in the inset of Fig. 4 represents time zero, where the TOC/TOC° ratio is close to 1 in S1, S2 and S3. This confirms that the WSF was initially homogeneously distributed in the electrochemical cell. The results indicate that ER affects not only the amount of WSO generated but also their spatial distribution within the sediment bed. Notably, after ER, higher concentrations of WSO were present in all sediment sections and for all investigated *E* values, as indicated by TOC/TOC° ratios consistently greater than 1. Thus, showing that ER induces the transformation of TPHs and PAHs into more soluble water organics (which increase the TOC in the pore water). As shown in Fig. 4, the *E* affects strongly both the TOC/TOC° ratios (and consequently the SWO amount) and the spatial distribution of TOC as described in the follow.

- The amount of WSO increased generally with the *E* values, where higher reaction rates were observed. For example, at 0.05, 0.25 and 1.00 V cm^{-1}, the average TOC/TOC° ratios were 2.50, 5.30 and 14.2, respectively.
- The spatial distribution depended on *E*. For $E < 0.25$ V cm^{-1} the TOC/TOC° ratio increased progressively from S3 to S2 and S1 (Fig. 4). As an example, the TOC/TOC° ratio at 0.15 V cm^{-1} was 7.00, 6.10 and 5.60 in S1, S2, and S3, respectively. Overall, an opposite trend of the spatial distribution was observed for higher *E*. For example, at 0.50 or 1.00 V cm^{-1}, the ratios were 2.60, 7.00, and 38.0 or 3.00, 11.9, and 27.6 in S1, S2, and S3, respectively.

On overall, these data confirm that ER does not induces only transport phenomena but gives rise also to relevant chemical transformations of organic pollutants, whose extent depends strongly on adopted *E*, changing the soil-water repartition of organics.

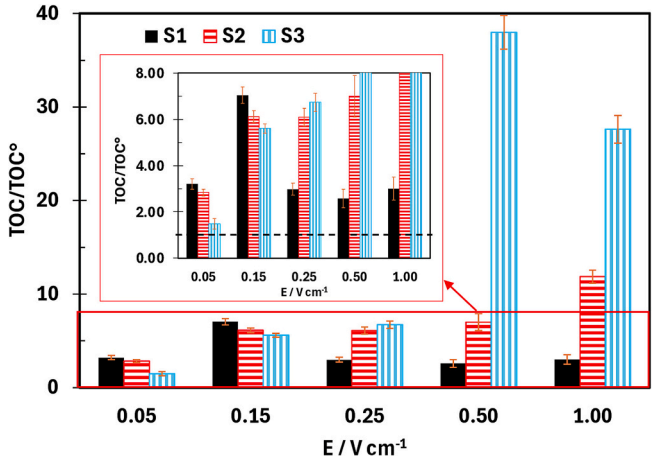

Fig. 4. Effect of *E* ranged from 0.05 to 1.00 V cm^{-1} on the normalized TOC/TOC° in the section S1, S2 and S3 after 96 h of electrochemical treatment. TOC is the total organic carbon measured by TOC analyzer. Error bars indicate the standard deviation calculated from two independent experiments. The insert shows the zoom of TOC/TOC° (y-axis) between 0 and 8. The dashed black line in the insert's figure represents the zero time where the TOC/TOC° ratio is ~1.

3.3.2. Nature of the identified soluble water organics

According to the literature, the oxidation pathways of organic compounds (TPHs and/or PAHs) in Cl^-–containing aqueous electrolytes lead to the formation of phenolic compounds (phenol and chlorophenols), chloroacetic acids (CAAs), and low-molecular-weight products, such as carboxylic acids (CAs) [46–49]. Based on this information and the TOC results, a series of analyses was planned to characterize the nature of these water-soluble compounds. Fig. 5A and B show the final concentrations of CAAs and CAs, respectively, detected in the pore water after ER under the investigated values of *E*. Overall, these results show that, under all adopted conditions, both CAAs and CAs were in situ generated from the ER of TPHs and PAHs contaminated marine sediments.

In the case of CAAs, monochloroacetic acid, dichloroacetic acid and trichloroacetic acid were detected. The total CAAs content increased with the applied *E* (Fig. 5A) likely due to the stronger driving force promoting electrochemical reactions. This enhanced driving force may accelerate the formation of chlorinated oxidants and, consequently, the production of CAAs. The applied *E* also influenced their spatial distribution (Fig. 5A): *i*) at 0.05 V cm^{-1}, CAAs were distributed more uniformly across S1, S2 and S3; *ii*) at 0.15 and 0.25 V cm^{-1}, their concentration increased from S1 to S3; and, *iii*) for $E \geq 0.50$ V cm^{-1}, their concentration increased from S3 to S1. Several factors may explain these patterns. Based on the final pH values (Fig. 3), CAAs are expected to be present in their anionic forms (see pK_{a1} in Table S1 of the Supplementary Material). Once generated within the sediment bed, these negatively charged species would preferentially migrate toward the positive electrode via electromigration, leading to the accumulation of CAAs content in section S1. This mechanism supports the trends observed for relatively high *E* ($\geq$ 0.50 V cm^{-1}) and aligns with the stronger oxidative conditions near the anode (S1), which can further promote CAAs formation. By contrast, the opposite trends observed for lower *E* values may be attributed to CAAs being transported primarily by electroosmotic flow rather than electromigration under those conditions, resulting in their accumulation near S3.

For the CAs, oxalic acid, formic acid and tartaric acid were identified as the major compounds, with oxalic acid consistently detected at the highest concentrations. As in the case of CAAs, the highest CAs content were detected at the highest applied *Es* (Fig. 5B) likely due to the stronger driving force promoting electrochemical reactions. For most of the *E*s, the content of CAs increases from S1 to S3, except under 0.05 V cm^{-1}. Under the latter case, the opposite trend was observed: CAs' content increases from S3 to S1. Moreover, the differences in CAs content among S1, S2, and S3 became more pronounced as *E* increased. These trends can be explained by considering both the enhanced reduction rates and the pH variations induced by the applied *E*. Based on the measured pH values (Fig. 3), CAs are also expected to occur predominantly in their anionic forms (see pK_{a1} and pK_{a2} in Table S1 of the Supplementary Material). Thus, at the lowest *E* (0.05 V cm^{-1}), once formed, these anionic species preferentially migrate toward the positive electrode via electromigration, which is consistent with the elevated CAs levels noted in section S1. For $E \geq 0.15$ V cm^{-1}, the reversal of this trend can be attributed to two concurrent effects: *i*) the combined influence of electromigration driving CAs toward the anode and electroosmotic flow transporting them toward the cathode (an effect that is expected becomes stronger with increasing *E*) and *ii*) the further oxidation of CAs occurring near the anode, which intensifies at higher *E*. In fact, the CAs content measured in S1 decreases with increasing *E* (Fig. 5B). This different pattern with respect to the CAAs could be corroborated to the fact the CAs are easily to be oxidized than CAAs.

The pore water was also analysed with the aim to search phenols and chlorophenols, however, no phenol neither chlorophenols were detected at least under our detection limits (0.05 mg kg^{-1}).

Considering all these aspects, it is reasonable to conclude that, under

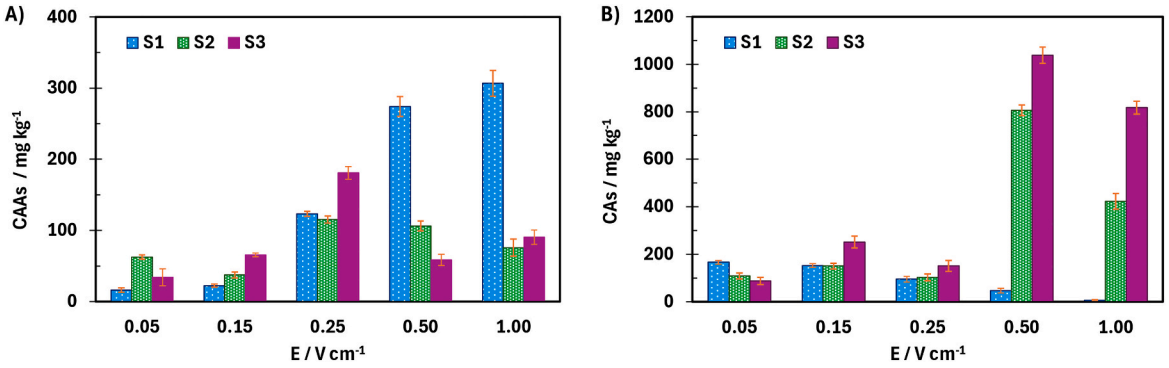

Fig. 5. Effect of *E* ranged from 0.05 to 1.00 V cm^{-1} on the (A) chloroacetic acids (CAAs) and (B) carboxylic acids (CAs) concentration (mg kg^{-1}) in the section S1, S2 and S3 after 96 h of electrochemical treatment. The identified CAAs were mono-, di- and tri- chloroacetic acids. The main identified CAs were oxalic, formic and tartaric acids. Error bars indicate the standard deviation calculated from two independent experiments.

the conditions adopted, the primary pathway for the removal of TPHs and PAHs from marine sediments involves the formation of higher amounts of WSO, including both CAAs and CAs.

The present findings are consistent with previous research. Numerous studies have shown that the electrochemical treatment of aromatic organic contaminants in chloride-containing aqueous media can give rise to unwanted halogenated organic by-products, generated through addition and substitution reactions involving active chlorine radicals and/or chlorine-derivates oxidants [33]. In line with this evidence, the CAAs and CAs detected here are unlikely to derive directly from PAHs or TPHs. Instead, they are plausibly produced as secondary oxidation products, formed when open-chain intermediates generated during contaminants degradation subsequently react with chlorinated species.

The appearance of CAAs in chloride-rich environments can be attributed to the electrochemical generation of active chlorine species from Cl^- inherently present in marine sediments, following mechanisms analogous to those reported for the anodic oxidation of aromatic compounds in aqueous NaCl solutions (eqs. 4–6) [46–49]. Under anodic conditions, chloride-based oxidants (Cl_2/HClO/OCl^-, depending on pH) act as strong electrophilic chlorinating agents [50]. They undergo electrophilic aromatic substitution on organic pollutants, attacking electron-rich positions and forming chlorinated aromatic intermediates through successive substitution steps [51]. Concurrently, active chlorine species may further react with these intermediates [52], promoting their oxidation and ring cleavage. This sequence of reactions ultimately leads to the formation of CAAs and CAs observed in this study [47].

It is important to underline that the environmental impact of converting these contaminants into CAAs and CAs depends strongly on their concentrations. The Predicted No-Effect Concentration (PNEC) of CAAs is extremely low in marine water and sediment (Table S2, SM); therefore, the release of these compounds into pore water should be strictly limited in situ. It is worth noting that CAAs exhibit well-documented ecotoxicological effects even at low concentrations. Literature reports show that exposure of submerged macrophytes to CAAs in the range of 1–100 μg/L significantly inhibits root and leaf growth and reduces chlorophyll content, with leaf elongation dropping to 44–67% of controls at 10–100 μg/L [53]. CAAs also alters oxidative stress biomarkers, causing marked increases in antioxidant enzymes (such us superoxide dismutase, SOD, and peroxidase, POD) activity and ultrastructural damage to leaf cells [53]. Although CAAs were formed at relatively low concentrations in this study, their intrinsic toxicity highlights the need to strictly limit their accumulation in situ. Importantly, this does not undermine the applicability of ER but rather emphasizes the importance of optimizing operating conditions (e.g., *E* intensity, electrode configuration, treatment duration, polarity management, or integrated approaches) to minimize byproduct formation and promote further oxidation toward mineralization. In contrast, CAs pose a lower environmental concern. For example, oxalic acid and tartaric acid are not classified as hazardous substances (Table S2, SM); while the PNEC of formic acid (Table S2, SM) is considerably higher than that of CAAs and POPs (Table 1). Nevertheless, elevated concentrations of formic acid have been reported to induce oxidative stress and acute toxicity in benthic invertebrates, such as *Tubifex tubifex*, indicating that its accumulation should also be avoided [54].

To evaluate the contribution of identified water-soluble byproducts to the total pool of generated WSO, the organic carbon (OC) associated with CAAs and CAs ($\%_{w/w}$) was estimated as a mass percentage ratio between the OC contribution of CAAs or CAs (mg_C kg^{-1}) and the increase in TOC measured in pore water (OC_{WSO}; mg_C kg^{-1}), as reported in detailed in the Supplementary Material. It was observed that CAAs– and CAs– OC fraction was 5.3 ± 3.0 and 18 ± 5.0%, respectively, under all the adopted operative conditions. The remaining fraction is due to other unidentified water-soluble organics. Indeed, it should also be acknowledged that the oxidative transformation of complex PAHs and TPHs mixtures may generate additional oxygenated intermediates not targeted in this study (e.g., aldehydes, ketones, short-chain organic acids, oxygenated PAHs [34–37]). It is worth to mention that unidentified products may exhibit distinct toxicological properties, and their presence could influence the overall environmental relevance of the treatment. Future work should therefore include broader analytical screening (to capture a more complete spectrum of transformation products and to support a more comprehensive evaluation of toxicity and detoxification pathways associated with ER treatments) and extended or advanced ER strategies aimed at achieving total mineralization to CO_2 while preserving sediment integrity and minimizing the release of transformation products into pore water.

To address the scalability and field applicability of the proposed ER approach, the following considerations are provided. While the present results are derived from laboratory-scale experiments, factors such as the thickness of the contaminated layer, high salinity, porewater movement, seasonal temperature variations, and seabed disturbance may influence *E* distribution and contaminant transport under real conditions. Several potential engineering strategies will be required to ensure effective scale-up, including: *i*) modular or vertically distributed durable electrodes to maintain homogeneous *E* propagation across deeper or spatially heterogeneous sediment layers; *ii*) staged or pulsed treatments to limit excessive current density, local heating, gas formation, and by-product accumulation; and *iii*) simple hydraulic controls (e.g., barriers or silt screens) to minimize the dispersion of soluble intermediates. In marine sediments, additional site-specific aspects such as bioturbation, sediment consolidation, and shear strength should also be considered when evaluating prolonged ER operation. Although the low *E* intensities and current densities adopted here are expected to minimize physical disturbance, electrolysis of saline pore water may locally generate gaseous products (e.g., O_2, H_2, and, in chloride-rich

environments, Cl_2), which could affect sediment porosity or micro-scale structure if not properly dissipated. Similarly, while graphite electrodes exhibit high chemical and mechanical stability under low-*E* conditions, long-term exposure may lead to surface fouling or changes at the electrode–sediment interface, potentially influencing current distribution. These considerations highlight the importance of optimized electrode configuration, gas dissipation pathways, and ecological monitoring to preserve sediment integrity and benthic habitats. Pilot-scale studies will be essential to assess electrode durability, gas management, and sediment physical stability under dynamic marine conditions.

4. Conclusions

In this work, real marine sediments from Bagnoli-Coroglio Bay (Naples, Italy) contaminated with TPHs and PAHs were treated by an electrochemical process under a wide range of *E* (0.05–1.00 V cm^{-1}) over 96 h, using electrodes placed in direct contact with the sediments and without adding enhancing agents. This study demonstrates that ER simultaneously promotes both the in situ mobilization and chemical transformation of contaminants, even under mild operating conditions. In particular, the spatial redistribution of TPHs and PAHs confirms that ER induces mobilization even at low *E* values. At the same time, measurable removal of TPHs and PAHs, together with the increase in TOC in pore water and the formation of chloroacetic and carboxylic acids, indicates that ER promotes the contaminants' chemical transformation into more water-soluble organics. More specifically, both mobilization and transformation were strongly influenced by *E*, revealing a non-linear trend with a minimum at 0.25 V cm^{-1}. Appreciable removals were obtained at both ends of the investigated *E* range (0.05 and 1.00 V cm^{-1}), with PAHs consistently showing higher abatement than TPHs.

Overall, the results show that ER is an effective strategy for treating real marine sediments, enabling the simultaneous in situ mobilization and chemical transformation of organic contaminants, tuneable by the applied *E*. Future studies should focus on the optimization of ER conditions to maximize treatment efficiency and minimize toxic water soluble organics preserving sediment integrity and avoiding the release of organics into the water column. Moreover, given the very high initial contaminant concentrations relative to sediment quality guideline values, the removals achieved in this study should not be interpreted as sufficient, by themselves, to ensure regulatory compliance. Future work should therefore include broader analytical screening (to capture a more complete spectrum of transformation products and to support a more comprehensive evaluation of toxicity and detoxification pathways associated with ER treatments) and extended or advanced ER strategies aimed at achieving total mineralization to CO_2 while preserving sediment integrity and minimizing the release of transformation products into pore water.

CRediT authorship contribution statement

Federica Proietto: Writing – review & editing, Writing – original draft, Visualization, Supervision, Methodology, Funding acquisition, Data curation, Conceptualization. **Paola Meli:** Investigation, Data curation. **Andrea Di Franco:** Formal analysis, Data curation. **Flavia Gianfolcaro:** Investigation, Data curation. **Fabio D'Agostino:** Formal analysis, Data curation. **Alessandro Galia:** Funding acquisition. **Onofrio Scialdone:** Writing – review & editing, Visualization, Supervision.

Declaration of competing interest

The authors declare that they have no known competing financial interests or personal relationships that could have appeared to influence the work reported in this paper.

Acknowledgements

The partial financial support of project Next Generation EU" - PNRR M4 - C2 -investimento 1.1: Fondo per il Programma Nazionale di Ricerca e Progetti di Rilevante Interesse Nazionale (PRIN) - PRIN 2022PNRR cod. P2022AK3CA title "Sustainable rEmedial Approach FoR pOlluted mariNe sedimenTs (SEAFRONT)" CUP B53D23033560001, and of the University of Palermo are gratefully acknowledged.

Appendix A. Supplementary data

Supplementary data to this article can be found online at https://doi.org/10.1016/j.cej.2026.174823.

Data availability

Data will be made available on request.

References

[1] G. Lofrano, G. Libralato, D. Minetto, S. De Gisi, F. Todaro, B. Conte, D. Calabrò, L. Quatraro, M. Notarnicola, In situ remediation of contaminated marine sediment: an overview, Environ. Sci. Pollut. Res. 24 (2017) 5189–5206, https://doi.org/10.1007/s11356-016-8281-x.
[2] W. Chen, T. Xie, X. Li, R. Wang, Thinking of construction of soil pollution prevention and control technology system in China, Acta Pedol. Sin. 55 (2018) 557–568, https://doi.org/10.11766/trxb201711300488.
[3] T. Gereslassie, A. Workineh, O.J. Atieno, J. Wang, Determination of occurrences, distribution, health impacts of organochlorine pesticides in soils of central China, Int. J. Environ. Res. Public Health 16 (2019), https://doi.org/10.3390/ijerph16010146.
[4] L. Huysegoms, V. Cappuyns, Critical review of decision support tools for sustainability assessment of site remediation options, J. Environ. Manag. 196 (2017) 278–296, https://doi.org/10.1016/j.jenvman.2017.03.002.
[5] S. Ronchi, S. Salata, A. Arcidiacono, E. Piroli, L. Montanarella, Policy instruments for soil protection among the EU member states: a comparative analysis, Land Use Policy 82 (2019) 763–780, https://doi.org/10.1016/j.landusepol.2019.01.017.
[6] Y. Song, D. Hou, J. Zhang, D. O'Connor, G. Li, Q. Gu, S. Li, P. Liu, Environmental and socio-economic sustainability appraisal of contaminated land remediation strategies: a case study at a mega-site in China, Sci. Total Environ. 610–611 (2018) 391–401, https://doi.org/10.1016/j.scitotenv.2017.08.016.
[7] E. Romano, L. Bergamin, M. Celia Magno, G. Pierfranceschi, A. Ausili, Temporal changes of metal and trace element contamination in marine sediments due to a steel plant: the case study of Bagnoli (Naples, Italy), Appl. Geochem. 88 (2018) 85–94, https://doi.org/10.1016/j.apgeochem.2017.05.012.
[8] E. Romano, L. Bergamin, I.W. Croudace, G. Pierfranceschi, G. Sesta, A. Ausili, Measuring anthropogenic impacts on an industrialised coastal marine area using chemical and textural signatures in sediments: a case study of Augusta Harbour (Sicily, Italy), Sci. Total Environ. 755 (2021) 142683, https://doi.org/10.1016/j.scitotenv.2020.142683.
[9] G. Armiento, M. Barsanti, R. Caprioli, S. Chiavarini, F. Conte, C. Crovato, M. De Cassan, I. Delbono, M.R. Montereali, E. Nardi, L. Parrella, M. Pezza, M. Proposito, J. Rimauro, A. Schirone, F. Spaziani, Heavy metal background levels and pollution temporal trend assessment within the marine sediments facing a brownfield area (Gulf of Pozzuoli, Southern Italy), Environ. Monit. Assess. 194 (2022), https://doi.org/10.1007/s10661-022-10480-3.
[10] M. Buccino, M. Daliri, M. Calabrese, R. Somma, A numerical study of arsenic contamination at the Bagnoli bay seabed by a semi-anthropogenic source. Analysis of current regime, Sci. Total Environ. 782 (2021) 146811, https://doi.org/10.1016/j.scitotenv.2021.146811.
[11] D. Rosestolato, R. Bagatin, S. Ferro, Electrokinetic remediation of soils polluted by heavy metals (mercury in particular), Chem. Eng. J. 264 (2015) 16–23, https://doi.org/10.1016/j.cej.2014.11.074.
[12] D. Han, X. Wu, R. Li, X. Tang, S. Xiao, M. Scholz, Critical review of electro-kinetic remediation of contaminated soils and sediments: mechanisms, performances and technologies, Water Air Soil Pollut. 232 (2021), https://doi.org/10.1007/s11270-021-05182-4.
[13] K.R. Reddy, C. Cameselle, Electrochemical Remediation Technologies for Polluted Soils, Sediments and groundwater, John Wiley & Sons, Inc., Hoboken, New Jersey, 2009.
[14] F. Proietto, A. Khalil, W. Maouch, A. Galia, O. Scialdone, Electrochemical remediation of phenol contaminated kaolin under low-strength electric fields, Environ. Technol. Innov. 32 (2023) 103286, https://doi.org/10.1016/j.eti.2023.103286.
[15] L.M. Zanko, J.K. Wittle, S. Pamukcu, Case study: Electrochemical Geo-Oxidation (ECGO) treatment of Massachusetts New Bedford Harbor sediment PCBs, Electrochim. Acta 354 (2020) 136690, https://doi.org/10.1016/j.electacta.2020.136690.
[16] A.B. Fardin, A. Jamshidi-Zanjani, A critical review on soil remediation using electrokinetic-enhanced permeable reactive barriers: challenges and

enhancements, Chem. Eng. J. Adv. 23 (2025) 100774, https://doi.org/10.1016/j.ceja.2025.100774.
[17] A. Saini, D.N. Bekele, S. Chadalavada, C. Fang, R. Naidu, Electrokinetic remediation of petroleum hydrocarbon contaminated soil (I), Environ. Technol. Innov. 23 (2021) 101585, https://doi.org/10.1016/j.eti.2021.101585.
[18] F. Proietto, P. Meli, C. Prestigiacomo, A. Galia, O. Scialdone, Study of electrochemical remediation of clay spiked with C12-C18 alkanes, J. Environ. Chem. Eng. 12 (2024) 111780, https://doi.org/10.1016/j.jece.2023.111780.
[19] F. Proietto, F. D'Agostino, M. Bonsignore, M. Del Core, M. Sprovieri, A. Galia, O. Scialdone, Electrochemical remediation of synthetic and real marine sediments contaminated by PAHs, Hg and As under low electric field values, Chemosphere 350 (2024) 141009, https://doi.org/10.1016/j.chemosphere.2023.141009.
[20] R. Fan, S. Guo, T. Li, F. Li, X. Yang, B. Wu, Contributions of electrokinetics and bioremediation in the treatment of different petroleum components, Clean (Weinh) 43 (2015) 251–259, https://doi.org/10.1002/clen.201300659.
[21] E. Ferrarese, G. Andreottola, Application of electrochemical techniques for the remediation of soils contaminated with organic pollutants, in: Association for Environmental Health and Sciences - 23rd Annual International Conference on Soils, Sediments and Water 2007 13, 2007, pp. 343–372.
[22] G. Andreottola, E. Ferrarese, Application of advanced oxidation processes and electrooxidation for the remediation of river sediments contaminated by PAHs, J. Environ. Sci. Health A Tox. Hazard. Subst. Environ. Eng. 43 (2008) 1361–1372, https://doi.org/10.1080/10934520802231990.
[23] K. Johansson, A. Ruiz-Valencia, I. Carabante, T.M. Vogel, E. Lindberg, J. Kumpiene, Electrochemical oxidation of polycyclic aromatic hydrocarbons in soil co-contaminated with arsenic, J. Environ. Manag. 388 (2025), https://doi.org/10.1016/j.jenvman.2025.125978.
[24] F. Proietto, V. Musacchia, C. Prestigiacomo, A. Galia, New insights on electrochemical remediation of soil / sediments: in situ phenol transformation and mineralization in spiked kaolin under low electric fields, Environ. Technol. Innov. 40 (2025) 104576, https://doi.org/10.1016/j.eti.2025.104576.
[25] P.P. Falciglia, D. Malarbì, V. Greco, F.G.A. Vagliasindi, Surfactant and MGDA enhanced – electrokinetic treatment for the simultaneous removal of mercury and PAHs from marine sediments, Sep. Purif. Technol. 175 (2017) 330–339, https://doi.org/10.1016/j.seppur.2016.11.046.
[26] P.P. Falciglia, D. Malarbì, R. Maddalena, V. Greco, F.G.A. Vagliasindi, Remediation of Hg-contaminated marine sediments by simultaneous application of enhancing agents and microwave heating (MWH), Chem. Eng. J. 321 (2017) 1–10, https://doi.org/10.1016/j.cej.2017.03.097.
[27] P. Guedes, V. Lopes, N. Couto, E.P. Mateus, C.S. Pereira, A.B. Ribeiro, Electrokinetic remediation of contaminants of emergent concern in clay soil: effect of operating parameters, Environ. Pollut. 253 (2019) 625–635, https://doi.org/10.1016/j.envpol.2019.07.040.
[28] T. Maqbool, D. Jiang, Electrokinetic remediation leads to translocation of dissolved organic matter/nutrients and oxidation of aromatics and polysaccharides, Sci. Total Environ. 876 (2023) 162703, https://doi.org/10.1016/j.scitotenv.2023.162703.
[29] D.D. MacDonald, C.G. Ingersoll, T.A. Berger, Development and evaluation of consensus-based sediment quality guidelines for freshwater ecosystems, Arch. Environ. Contam. Toxicol. 39 (2000) 20–31, https://doi.org/10.1007/s002440010075.
[30] M. Muscetta, F. Bianco, G. Trancone, M. Race, A. Siciliano, F. D'Agostino, M. Sprovieri, L. Clarizia, Washing bottom sediment for the removal of arsenic from contaminated Italian coast, Processes 11 (2023), https://doi.org/10.3390/pr11030902.
[31] A.R. Ferreira, P. Guedes, E.P. Mateus, A.B. Ribeiro, N. Couto, Emerging organic contaminants in soil irrigated with effluent: electrochemical technology as a remediation strategy, Sci. Total Environ. 743 (2020), https://doi.org/10.1016/j.scitotenv.2020.140544.
[32] S. Pamukcu, Electrochemical technologies for petroleum contaminated soils, in: M. A. Rodrigo, E.V. Dos Santos (Eds.), Electrochemically of Contaminated Remediation Assisted Soils., Springer, 2021, pp. 455–484, https://doi.org/10.1007/978-3-030-68140-1_18.
[33] O. Scialdone, F. Proietto, A. Galia, Electrochemical production and use of chlorinated oxidants for the treatment of wastewater contaminated by organic pollutants and disinfection, Curr. Opin. Electrochem. 27 (2021) 100682, https://doi.org/10.1016/j.coelec.2020.100682.
[34] X. Bai, H. Sun, J. Sun, Z. Zhu, Efficient removal of sixteen priority polycyclic aromatic hydrocarbons from textile dyeing sludge using electrochemical Fe2+-activated peroxymonosulfate oxidation-a green pretreatment strategy for textile dyeing sludge toxicity reduction, J. Hazard. Mater. 435 (2022) 129087, https://doi.org/10.1016/j.jhazmat.2022.129087.
[35] D.S. Cordeiro, P. Corio, Electrochemical and photocatalytic reactions of polycyclic aromatic hydrocarbons investigated by Raman spectroscopy, J. Braz. Chem. Soc. 20 (2009) 80–87, https://doi.org/10.1590/S0103-50532009000100014.
[36] X. Chen, S. Mu, Y. Luo, Degradation of petroleum pollutants in oil-based drilling cuttings using an Fe2+-based Fenton-like advanced oxidation processes, Environ. Sci. Pollut. Res. 30 (2023) 37669–37678, https://doi.org/10.1007/s11356-022-24925-2.
[37] S. Adhami, A. Jamshidi-Zanjani, A.K. Darban, Remediation of oil-based drilling waste using the electrokinetic-Fenton method, Process. Saf. Environ. Prot. 149 (2021) 432–441, https://doi.org/10.1016/j.psep.2020.11.018.
[38] H. Ajab, M.H. Isa, A. Yaqub, Electrochemical oxidation using Ti/RuO2 anode for COD and PAHs removal from aqueous solution, Sustain. Mater. Technol. 26 (2020) e00225, https://doi.org/10.1016/j.susmat.2020.e00225.
[39] M.T. Alcántara, J. Gómez, M. Pazos, M.A. Sanromán, Combined treatment of PAHs contaminated soils using the sequence extraction with surfactant-electrochemical degradation, Chemosphere 70 (2008) 1438–1444, https://doi.org/10.1016/j.chemosphere.2007.08.070.
[40] J.M. de M. Henrique, J. Isidro, C. Saez, E.V. Dos Santos, M.A. Rodrigo, Enhancing electrokinetic soil flushing with air stripping for the treatment of soil polluted with phenol and o-chlorophenol, Electrochim. Acta 432 (2022), https://doi.org/10.1016/j.electacta.2022.141189.
[41] S. Lukman, M.H. Essa, N.D. Mu'Azu, A. Bukhari, Coupled electrokinetics-adsorption technique for simultaneous removal of heavy metals and organics from saline-sodic soil, Sci. World J. 2013 (2013), https://doi.org/10.1155/2013/346910.
[42] N. Garcia-blas, E. Jimenez-relinque, R. Nevshupa, M. Castellote, Electrokinetic approach to assess the behaviour of a contaminated marine sediment, 2020.
[43] Y.B. Acar, R.J. Gale, A.N. Alshawabkeh, R.E. Marks, S. Puppala, M. Bricka, R. Parker, Electrokinetic remediation: basics and technology status, J. Hazard. Mater. 40 (1995) 117–137, https://doi.org/10.1016/0304-3894(94)00066-P.
[44] D. Rahner, G. Ludwig, J. Röhrs, Electrochemically induced reactions in soils - a new approach to the in-situ remediation of contaminated soils? Part 1: the microconductor principle, Electrochim. Acta 47 (2002) 1395–1403, https://doi.org/10.1016/S0013-4686(01)00854-4.
[45] J. Röhrs, G. Ludwig, D. Rahner, Electrochemically induced reactions in soils - a new approach to the in-situ remediation of contaminated soils? Part 2: remediation experiments with a natural soil containing highly chlorinated hydrocarbons, Electrochim. Acta 47 (2002) 1405–1414, https://doi.org/10.1016/S0013-4686(01)00855-6.
[46] A.Y. Bagastyo, J. Radjenovic, Y. Mu, R.A. Rozendal, D.J. Batstone, K. Rabaey, Electrochemical oxidation of reverse osmosis concentrate on mixed metal oxide (MMO) titanium coated electrodes, Water Res. 45 (2011) 4951–4959, https://doi.org/10.1016/j.watres.2011.06.039.
[47] Y. Hao, H. Ma, F. Proietto, C. Prestigiacomo, P. Ma, A. Galia, O. Scialdone, Removal of phenol from water in the presence of NaCl in undivided cells equipped with carbon felt or Ni cathodes: effect of air pressure, ChemElectroChem 9 (2022) 3–9, https://doi.org/10.1002/celc.202200091.
[48] J.T. Jasper, Y. Yang, M.R. Hoffmann, Toxic byproduct formation during electrochemical treatment of latrine wastewater, Environ. Sci. Technol. 51 (2017) 7111–7119, https://doi.org/10.1021/acs.est.7b01002.
[49] H. Zöllig, A. Remmele, C. Fritzsche, E. Morgenroth, K.M. Udert, Formation of chlorination byproducts and their emission pathways in chlorine mediated electro-oxidation of urine on active and nonactive type anodes, Environ. Sci. Technol. 49 (2015) 11062–11069, https://doi.org/10.1021/acs.est.5b01675.
[50] C. Prasse, U. Von Gunten, D.L. Sedlak, Chlorination of phenols revisited: unexpected formation of α,β-unsaturated C4-dicarbonyl ring cleavage products, Environ. Sci. Technol. 54 (2020) 826–834, https://doi.org/10.1021/acs.est.9b04926.
[51] M. Deborde, U. von Gunten, Reactions of chlorine with inorganic and organic compounds during water treatment-kinetics and mechanisms: a critical review, Water Res. 42 (2008) 13–51, https://doi.org/10.1016/j.watres.2007.07.025.
[52] X. Li, Y. Su, R. Bai, Q. Li, Effect of chloride ions on the degradation of phenol and the formation of chlorinated byproducts in BDD and RuO2-IrO2/Ti anode systems, J. Environ. Chem. Eng. 13 (2025) 119089, https://doi.org/10.1016/j.jece.2025.119089.
[53] K. Huang, H. Huang, X. Huang, A. Lao, Z. Zheng, H. Wu, Combined toxic effects and mechanisms of chloroacetic acid and N-nitrosodimethylamine on submerged macrophytes, Water (Basel) 16 (2024) 2689, https://doi.org/10.3390/w16182689.
[54] P. Garai, P. Banerjee, P. Sharma, A. Chatterjee, R. Bhattacharya, N.C. Saha, Mechanistic insights to lactic and formic acid toxicity on benthic oligochaete worm Tubifex tubifex, Environ. Sci. Pollut. Res. 29 (2022) 87319–87333, https://doi.org/10.1007/s11356-022-21361-0.